Role of probe design and bioassay configuration in surface enhanced Raman scattering based biosensors for miRNA detection

Role of probe design and bioassay configuration in Surface Enhanced Raman Scattering based biosensors for miRNA detection

Chiara Novara[a*], *Daniel Montesi*[a], *Sofia Bertone*[a], *Niccolò Paccotti*[a], *Francesco Geobaldo*[a], *Marwan Channab*[a,b], *Angelo Angelini*[b], *Paola Rivolo*[a], *Fabrizio Giorgis*[a], *Alessandro Chiadò*[a]

[a]*Department of Applied Science and Technology, Politecnico di Torino, Corso Duca degli Abruzzi, 24, 10129 Turin, Italy.*

[b]*Advanced Materials and Life Sciences, Istituto Nazionale di Ricerca Metrologica (INRiM), Strada delle Cacce 91, Turin 10135, Italy.*

*Corresponding author, e-mail chiara.novara@polito.it, phone: 0110904713

KEYWORDS: Surface Enhanced Raman Scattering, miRNAs, Raman reporters, hot-spots, distance-dependent near field coupling, biosensors, metal-dielectric plasmonic nanostructures

ABSTRACT. The accurate design of labelled oligo probes for the detection of miRNA biomarkers by Surface Enhanced Raman Scattering (SERS) may improve the exploitation of the plasmonic enhancement. This work, thus, critically investigates the role of probe labelling configuration on the performance of SERS-based bioassays for miRNA quantitation. To this aim, highly efficient SERS substrates based on Ag-decorated porous silicon/PDMS membranes are functionalized according to bioassays relying on a one-step or two-step hybridization of the target miRNA with DNA probes. Then, the detection configuration is varied to evaluate the impact of different Raman reporters and their labelling position along the oligo sequence on bioassay sensitivity. At high miRNA concentration (100-10 nM), a significantly increased SERS intensity is detected when the reporters are located closer to the plasmonic surface compared to farther probe labelling positions. Counterintuitively, a levelling-off of the SERS intensity from the different configurations is recorded at low miRNA concentration. Such effect is attributed to the increased relative contribution of Raman hot-spots to the whole SERS signal, in line with the electric near field distribution simulated for a simplified model of the Ag nanostructures. However, the beneficial effect of reducing the reporter-to-surface distance is partially retained for a two-step hybridization assay thanks to the less sterically hindered environment in which the second hybridization occurs. The study thus demonstrates an improvement of the detection limit of the two-step assay by tuning the probe labelling position, but sheds at the same time light on the multiple factors affecting the sensitivity of SERS-based bioassays.

1. Introduction

Surface Enhanced Raman Scattering (SERS) based sensors provide excellent results in the detection of biomolecules aimed to the easy and rapid diagnostics and follow-up monitoring of biomarkers.[1] Besides the development of tailored SERS active platforms, thanks to the improved knowledge on the SERS enhancement mechanisms and to the increased availability of synthetic procedures for Raman hot-spot engineering, the relevance of the functionalization strategy of the plasmonic nanostructures to enhance the sensitivity and the specificity of the detection has been fully recognized.[2] Actually, the use of specific capture probes anchored to the nanoparticles (NPs) surface is a widely adopted approach for biomarker detection, especially moving towards their analysis in complex mixtures such as biofluids or food extracts.[3,4] In such a framework, the direct detection of the analyte requires the processing of the complex spectral profiles by chemometric/machine learning tools[5] and is often challenging if very low concentrations need to be addressed. Moreover, the use of multiple probes in sandwich or competitive assays allowed introducing Raman reporters with a distinctive and intense Raman fingerprint.[4,6,7] The target biomolecule could thus be detected without the need of chemical modifications, but with an improved sensitivity thanks to the very high Raman cross section of the reporter, possibly excited in electronic resonance Raman conditions.

Among the multitude of interesting applications in biomedicine, microRNA (miRNAs) detection strategies are being deeply investigated.[8] Such short non-coding RNA strands regulate several biological processes through the control of gene expression and their dysregulation has been related to the onset of cancer.[9] Thus, miRNA profiling has a great potential for early tumour diagnosis, so that various approaches have been developed.[10] In such framework, SERS sensors provide good sensitivity, specificity, wide dynamic ranges and multiplexing capability at lower

cost and in shorter time compared to traditional analytical techniques[7,11,12]. To this aim, complementary DNA probes are usually grafted on plasmonic nanostructures. Recently, new protocols combined SERS with in situ amplification steps relying on the use of DNA cleaving or replicating enzymes or with on chip PCR.[13] Other works reported enzyme-free approaches[14], even [15]based on HCR (Hybridization Chain Reaction) amplification[11] or the use of SERS tags able to bind the captured miRNA sequence[6,16]. In such cases, the reported limits of detection are lowered down to the pM-fM concentration range, suitable for miRNA profiling in blood plasma[8], but the procedures are significantly complicated and featured by increased costs. Actually, the use of Raman reporters in miRNA detection assays is widespread and different probes were designed bearing the reporter in different position with respect to the plasmonic surface, such as in the case of ON-OFF assays based on the plasmonic enhancement variation upon a change of the surface to molecule distance at the opening of loop probes[17,18]; however, a critical comparison between different configurations was never considered. Indeed, an improvement of the analyte detection limits is envisaged if the 'plasmonic surface- Raman reporter' distance is reduced, due to the strong increase of SERS electromagnetic enhancement when the fluorophore-NPs spacing is decreased, together with a potential quenching of the deleterious photoluminescence yield of the reporter.[15]

In this work, we exploit the distance-dependence of the plasmonic enhancement to tune the performance of a SERS-based assay for the detection of miR-222, selected as a model miRNA because it is a recognized biomarker of various cancerous diseases, such as lung, brain, oral, prostatic, pancreatic, colorectal, renal, liver and haematological cancers[19–25]. Indeed, it is regarded as an oncogene that increases proliferation, survival and metastatic potential, modulating the clinical outcome in cancer patients[22,26,27]. The SERS analysis of this miRNA was evaluated through a detailed study of different detection configurations in which the distance of the reporter

from the nanostructured surface is varied. In order to widen the range of achievable spacings between the reporter and the metal surface, both a one-step and a two-step hybridization assays are tested using Ag-decorated porous silicon nanostructures as SERS active platform. The behaviour of each configuration versus miR-222 concentration is critically analysed and some unexpected trends, such as a reduced distance dependence of the SERS amplification at low target concentration, are understood in terms of the plasmonic properties of the SERS substrate and probe-target interaction at the silver surface.

2. Materials and methods

2.1 Synthesis and characterization of the SERS-active substrates

Ag-porous silicon (pSi)-polydimethylsiloxane (PDMS) membranes were prepared according to a previously reported procedure[28]. See the Supporting Information for the details.

2.2 Plasmonic properties simulation

A simplified model of the SERS active substrates consisting in Ag hemispheres dimers on pSi was modelled by 3D Finite Element Method (FEM). To this aim the *Electromagnetic Waves, Frequency Domain* module of the COMSOL Multiphysics software (version 5.1) was exploited. The excitation laser was simulated through a background electric field, E_{bk} = 1 V/m polarized along the axis of the two AgNPs at different wavelength, to study the coupling of their surface plasmons in resonant conditions. The electric near-field intensity in stationary conditions was calculated for representative NPs radius- inter-particle gap size combinations (radius: 12.5-15-17.5 nm; gap: 2-4-6-8 nm) and analysed inside and outside the inter-particle gap.

2.3 One-step and two-step hybridization assays

After a BSA pre-treatment step aimed to reduce non-specific binding[28], the SERS substrates were functionalized for miR-222 detection according to two previously optimized protocols[7]. In detail, for the one-step hybridization assay, a 5' thiol modified DNA probe (probe-222, all the used oligo sequences are reported in Table S1) complementary to the miR-222 sequence was immobilized on the surface of NPs, by overnight incubation in Tris-EDTA 1 M NaCl (TE NaCl pH 7.5) buffer at 4 μM concentration. A shorter sequence (half1) was instead used as capture probe for the two-step hybridization assay. The same immobilization conditions were employed (overnight incubation in TE NaCl pH 7.5), except for the concentration of half1 that was lowered to 2 μM. After the overnight incubation the sample were washed three times in TE supplemented with 0.05% tween20. The miR-222 hybridization was then performed in Sodium Saline Citrate 5x (SSC 5x) supplemented with 0.05% tween20. A Raman reporter-labelled miRNA was employed during the one-step hybridization assay. The unlabelled miRNA was instead used in the two-step hybridization assay, since the detection was allowed in the second hybridization step performed in SSC 5x supplemented with 0.05% tween20 and 1% BSA using a labelled probe (half2) complementary to the unpaired part of the miRNA sequence. After each step, three washings of 5 minutes were performed in appropriate buffers, as detailed elsewhere.[7] After that, the samples were quickly blow-dried in a nitrogen stream to avoid significant rearrangement of the oligonucleotides at the nanoparticles surface.

2.4 Detection configurations

Four configurations were studied. In detail, miR-222 was modified with a Raman reporter (R) at either the 5' or 3' terminus of the sequence in order to achieve significantly different reporter-to-

surface distances. Similarly, the half2 probe was labelled either at 3' or 5' end. To generalize the results, three reporters (Cyanine 3, Cyanine 5 and Rhodamine Green-X) differing in size and electronic absorption wavelength were used, evaluating the influence of steric hindrance and of the occurrence of resonance Raman effects. UCSF Chimera package (1.16)[29] was employed to prepare the graphical images and to evaluate the dimensions of the oligoprobe, including the alkanethiol spacer, by calculating the average value of at least three measurements on the 3D model structure, then to estimate the reporter-to-surface distances for each configuration. The performance of the configurations was investigated by the analysis of different miR-222 concentrations (100 nM, 50 nM, 25 nM, 10 nM, 5 nM, 2.5 nM, 1 nM, 0.5 nM, 0.25 nM, 0.1 nM) in buffer solutions, for the selected Raman reporters (12 different combinations as a whole). For each configuration the experiments were repeated at least three times.

2.5 Geometrical descriptors of the Raman reporters

Marvin Sketch (20.7.0, ChemAxon http://www.chemaxon.com) was used to draw and calculate the theoretical geometrical descriptors of the Raman reporters by means of the geometry tool, as reported elsewhere.[30] The input molecular structure for the reporters, depicted in Figure S1, includes the linkers used to conjugate the reporters with the oligonucleotide sequences. The Geometry Descriptors plug-in was used to estimate the following molecular parameters from these structures rendered in 3D as the lowest energy conformer and according to van der Waals atomic radii: (1) smallest/largest molecular surface projected from the 3D structure; (2) molecular length measured perpendicularly to this plane of projection; (3) molecular volume.

2.6 SERS analyses

All the SERS analyses were performed using a Renishaw InVia Raman microscope, equipped with a 514.5 nm laser line. The measurements were collected in backscattering configuration with a 100X long working distance objective (NA 0.75) and the laser power (100 mW) reduced to the 0.05 % through neutral density filters. A 5%-defocalization of the laser spot was applied to keep the power density as low as possible to avoid any oligonucleotide degradation. Each sample was analysed by recording a map of 100 spectra distributed over a grid of ca. 45 μm x 45 μm with a step size of 5 μm. The total acquisition time was 8 s for each spectrum, divided in 4 accumulations. The spectra were then analysed by a combination of the HyperSpec R package[31] and the Renishaw software WiRe 3.4. In detail, the baseline subtracted data set and the average spectrum of each map were calculated on R, while a deconvolution of selected regions of the spectra was carried out on WiRe 3.4 to obtain the integrated area value of specific Raman reporter bands considering Lorentzian line shapes for each recorded spectrum. The choice of the curves to be included in the fit was based on the typical bands of the reporter as well as on the Raman fingerprints of the oligo probe in the selected region. The curves were free to evolve within the posed constraints (peak height could not be negative, restricted Raman shift ranges around the typical band positions and limits to the band width). If the final peak height was 0, the band was considered absent. The intra-substrate variability was expressed in terms of Relative Standard Deviation (RSD).

The obtained integrated areas were used to build calibration curves (vibrational band area vs. miR-222 concentration) for the different configuration-reporter combinations. Linear regression was performed and the Limit of Detection (LOD) of the different methods were calculated as the concentration corresponding to the control sample value increased by three standard deviations, as described in the literature.[32]

3 Results and Discussion

Ag-decorated porous silicon-PDMS substrates were previously demonstrated as sensitive and reliable SERS platforms featured by a homogenous distribution of densely packed silver nanostructures[28] (a representative FESEM micrograph and an example of the analysis of the homogeneity of the SERS enhancement across the substrate surface are reported in Figure S2 and S3). In this study, such SERS substrates were thus selected for the comparison of the different detection configurations in the framework of miRNA analysis. Figure 1 depicts the investigated configurations, showing the last hybridization step of a one-step and a two-step hybridization assay.

Concerning the one-step assay, the miRNA is recognized by a fully complementary DNA probe immobilized at surface of AgNPs via a thiol group and two configurations are possible: one with the miRNA modified with a Raman reporter at the 5' terminus (miRNA R-5'), the other with the Raman reporter at the 3' terminus (miRNA R-3') (Figure 1a), namely bearing the reporter at the farthest end of the sequence or close to the NPs surface. The two-step assay, instead, has a great potential for the detection in real samples, since the target miRNA does not require chemical modification, as its specific recognition and detection are accomplished by two probes, each complementary to half of its sequence.

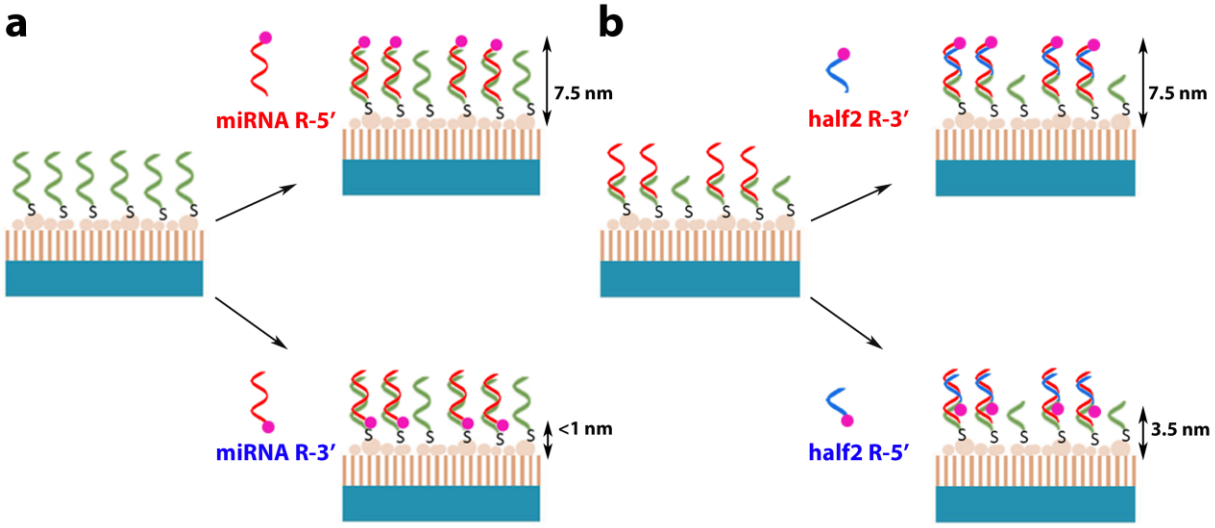

Figure 1. Scheme of the four detection configurations a) one-step assay: a fully complementary probe immobilized on the AgNPs binds the miRNA, which is labelled with a Raman reporter either at the 5' or 3' terminus; b) two-step assay: a first half-complementary probe (half1) immobilized on the AgNPs binds the unlabelled miRNA and the reporter is attached either at the 5' or 3' terminus of the half2 probe. The estimated reporter-to-surface distance for each configuration is highlighted. Note that NPs and oligos size are not to scale.

The thiolated "half1" probe is anchored to the NPs surface and captures the miRNA from the sample, while the sensitive detection occurs thanks to the subsequent hybridization of the "half2" probe conjugated to a Raman reporter. In analogy with the one-step assay, two configurations are available, having the reporter at the 5' (half2 R-5', close to the surface) or 3' (half2 R-3', far from the surface) terminus of the half2 probe (Figure 1b). Rhodamine Green-X (RGX, with absorption maximum at λ_{max} = 504 nm), Cyanine 3 (Cy3, λ_{max} = 550 nm) and Cyanine 5 (Cy5, λ_{max} = 648 nm) were identified as a convenient set of commercial reporters, suitable to compare the behaviour of the different configurations in the presence of electronic resonance (Cy3 and RGX) and with a varying size of the molecule.

In silico calculations were performed to obtain an estimation of the oligonucleotide length and thus of the distance of the reporter molecule from the surface. The maximum spacing was approximately 7.5 nm for the miRNA R-5' and half2 R-3' configurations, while the lowest one, calculated for miRNA R-3', was found below 1 nm. Instead, an intermediate distance of 3.5 nm was considered for the half2-5' configuration. All these calculations assumed that the hybridized complex was oriented perpendicularly to the NP surface, as widely accepted in the literature.[33,34] Indeed, this is a simplified model of DNA-particle and DNA-DNA interactions, since it is known that thiolated oligonucleotide monolayers can be arranged in tilted strands depending on the length of the oligonucleotide probe or of the alkanethiol spacer, on the probe density as well as on the metal towards the thiol is coordinated[35,36] and further complexity is given by the nanostructured surface.[37] A slightly shorter distance can be therefore expected. However, big tilt angles are unlikely in the studied system, as it was previously demonstrated that the SERS signal of the half1 probe and of probe-222 was almost identical[7], showing that their SERS spectra are dominated by the vibrational pattern of nucleobases belonging to the first part of the two sequences. This suggests that no significant tilting is occurring, as more nucleobases of the probe-222 would otherwise contribute to SERS pattern, due to the reduced distance from the surface.

To compare the SERS performance of the different configurations, the SERS substrates were then incubated according to the two functionalization protocols with the different miRNA R-3'/5' and half2 R-3'/5' sequences, varying the miR-222 concentration in the 100 nM-0.1 nM range.

3.1 One-step assay: miRNA R-5’ vs. miRNA R-3’

The average spectra of SERS maps obtained with the miR-222 RGX-3’/5’ are reported in Figure 2. An intense RGX vibrational pattern appears in the spectra of the samples incubated with a 100 nM miRNA concentration, overcoming any mode of the probe-222 down to 10 nM concentration.

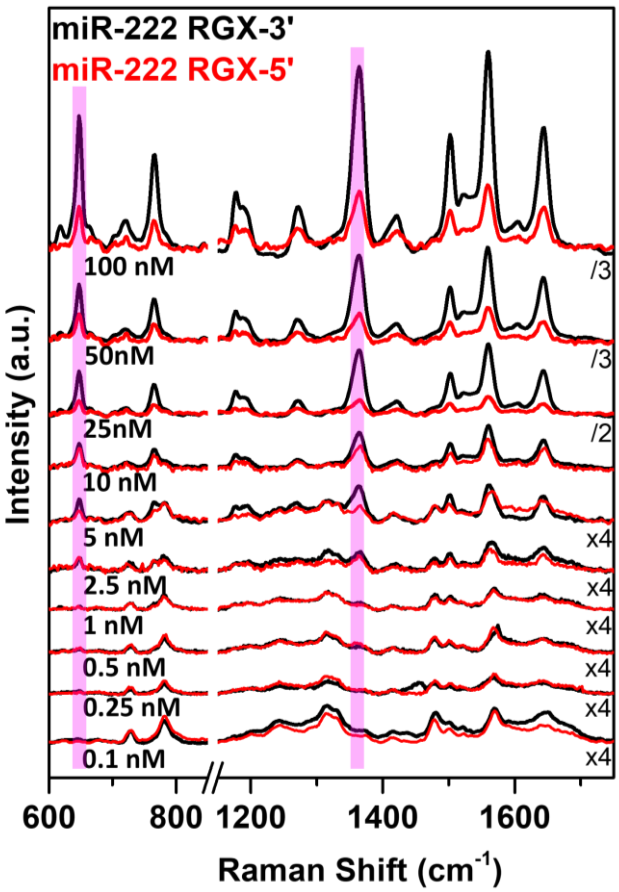

Figure 2. Average SERS spectra obtained from maps on the SERS substrates functionalized with the probe-222 according to the one-step hybridization protocol and incubated with different concentrations of miR-222 RGX-5’ (red curves) and miR-222 RGX-3’(black curves). The violet bars highlight two main bands of RGX (647 and 1364 cm^{-1}).

The typical C-C stretching of the xanthene ring at 1364 and 1646 cm^{-1} are clearly observed, together with all the characteristic bands of rhodamines, as assigned in Table S2. The isolated band around 647 cm^{-1}, attributed to the C-C ring in plane bending of the xanthene ring[38] modified with an additional carboxylic group, also shows a remarkable intensity and negligible superposition with the DNA probe bands. For this reason, such mode was selected to track the signal of all the RGX-labelled oligonucleotides, also for quantitative purposes. If the high concentration spectra of the two configurations are compared, the miRNA-RGX-3' SERS signal clearly exhibits a greater intensity compared to the configuration having the Raman reporter far from the NPs surface. Indeed, an enhancement of more than 3 times of the fluorophore signal is detected, explained by the increased electromagnetic field intensity due to the reduced distance from the NPs surface. Actually, some works investigated the distance-dependence of SERS intensity experimentally. The greatest drop of the plasmonic field intensity was shown to occur in the first nanometers (within 0-3 nm range from the metal surface, depending on the specific study), while for an increased spacing a slower decay was observed[36,39–41]. The fastest decay of the SERS intensity was observed in a high spacing resolution study by Masango et al. that reported a signal decrease to the 20% of the "in contact" one at 0.7 nm from the plasmonic surface.[39] Different experimental works agree instead on a SERS intensity decrease to the 7-10% of the zero-spacing signal at around 3-3.5 nm[39,41] and on its further five-fold decrease when the distance from the enhancing metal surface is raised from ~0.9 to ~7 nm[36,40].

However, a great variability is documented in such literature reports, especially concerning the slope of the SERS signal enhancement decrease in close proximity of the surface. Indeed, the derived distance-dependence of SERS enhancement may vary due to several factors, including the morphology of the employed SERS substrate and the nature of the spacing layer.[33,36] Despite this,

based on the available literature and taking into account a slight degree of uncertainty related to the orientation and position assumed by the reporter, the three-fold enhancement observed for the miRNA 3'-RGX configuration seems to be a reasonable result.

Similar conclusions can be drawn for the Cy3 reporter (SERS spectra at different miRNA concentrations can be found in Figure S4a), although the SERS intensity of the two configurations seems to differ in most of the cases by a factor higher than 4. Finally, in the case of the Cy5 reporter the strongest SERS intensity is still related to the close-to-the-surface Cy5 configuration. The differences in the SERS intensity provided by the miRNA-Cy5-5' and the miRNA-Cy5-3' (Figure S4b) are however reduced, compared to the resonantly excited reporters. The described behaviours can be appreciated by monitoring one of the main SERS bands of the two indocarbocyanine molecules, the vibrational mode located at around 1464 cm^{-1}, attributed to the CH_3 deformation of the ring substituents[42] (see Table S2 for a more complete assignment of the vibrational pattern of Cy3 and Cy5). It should be finally noted that the coupling of an emitting fluorophore with a plasmonic NP also affects the typical fluorescence of the dye. Indeed, an enhancement or a quenching of the fluorescence of the molecule can occur depending on the NP-dye separation, with the second contribution becoming dominant at few nanometres from the NP surface.[43] Accordingly, for the resonantly excited RGX and Cy3, the raw SERS spectra of the 5' configurations are characterized by a strong fluorescence background (Figure S5), yielding a greater shot noise[44] compared to the 3' one. Such fluorescence is instead significantly quenched when the reporter is close to the metal surface. A minor contribution of the improved signal-to-noise ratio to the whole SERS intensity increase for the 3' configuration cannot thus be excluded.

As a general trend, it can be further noticed that the difference in terms of SERS intensity between the close and far-to-the-surface configurations tends to decrease by lowering the miRNA

concentration, especially below 10 nM (the SERS spectra of miRNA RGX-5' and miRNA RGX-3' in the 5-0.1 nM concentration range are superimposed in Figure S6), sometimes fading for the lowest concentrations. The comparison between the calibration curves obtained for the 3' and 5' configurations reported in Figure 3 clearly highlight such a phenomenon, showing that the error bars of datapoints at low miR-222 concentration often overlap. Actually, statistical analysis based on the F-test (full details and results are available in Table S3 in the supplementary material) for the comparison of two data distributions reveals that differences between the two configurations

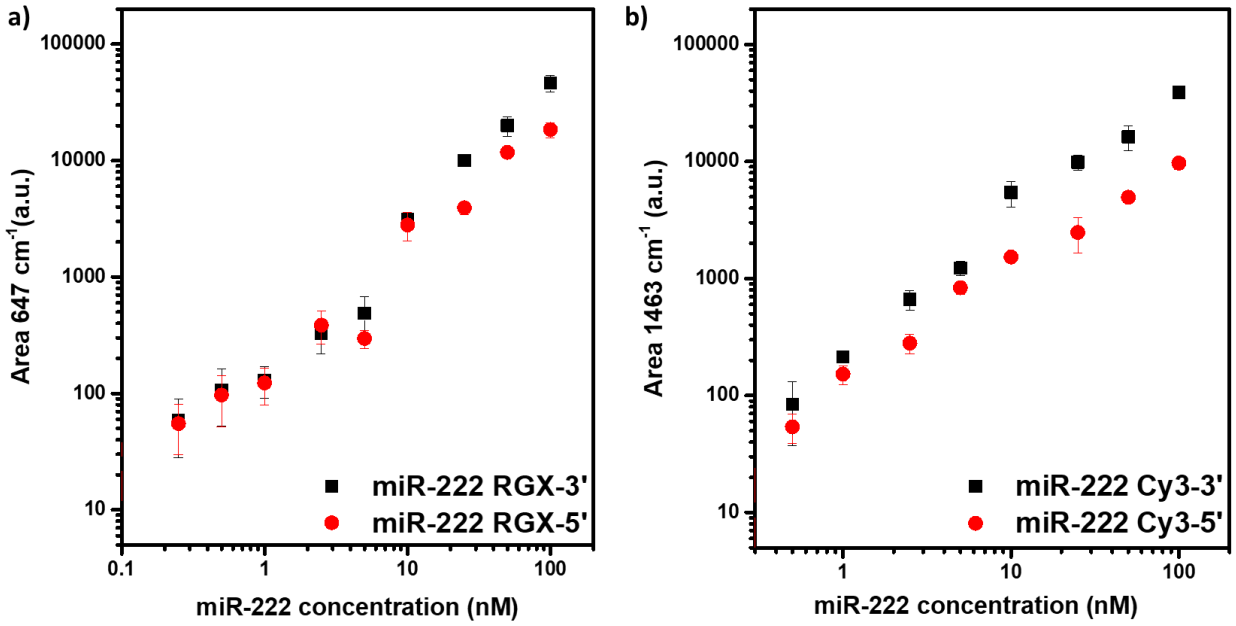

Figure 3. Average area of the main vibrational band of the miR-222 R-5'/3' vs. miR-222 concentration obtained by SERS mapping of the SERS substrates functionalized according to the one-step assay. a) RGX and b) Cy3 were employed as Raman reporters. Black squares represent the close-to-the-surface (3') configuration, while red circles the far-from-the-surface (5') one. The error bars correspond to the standard deviations of 100 SERS measurements.

are not statistically significant at 95% confidence level in the case of RGX, while such hypothesis has to be rejected for Cy3, but with a quite high p-value (0.031). This outcome is also reflected into the calculated LODs reported in Table 1 (all the calibration curves used for the calculation of the LODs are shown in Figure S7). Surprisingly, the LOD appears comparable for the Cy3-labelled miRNAs and even slightly lower for the miR-222 RGX-5' compared to the miR-222 RGX-3'. Such unexpected result depends however on the range of concentrations selected for the calculation. Indeed, a linear regime was identified for the Cy3 and RGX below 25 nM, so that for most of the calibration curves the linear regression was performed between 10 nM and 0 nM, including several low concentrations data points.

It should be finally noted that Cy5, spectrally excited far from its electronic absorptance, allows the detection of the target miRNA only for the medium-high concentrations (Table 1). Even in this case, the SERS intensity is clearly higher for the miRNA Cy5-3' compared to the miRNA Cy5-5'down to the 25 nM concentration (Figure S8), but the LOD is comparable for the two configurations.

Table 1. Limits Of Detection for the one-step assay performed by exploiting the six different configurations along with the miR-222 concentration ranges used for the linear regression.

	RGX		Cy3		Cy5	
	3'	5'	3'	5'	3'	5'
Linear range (nM)	0 - 5	0 - 2.5	0 - 5	0 - 10	0- 50	0-50
R^2	0.974	0.961	0.980	0.978	0.994	0.986
LOD (nM)	0.346	0.324	0.285	0.301	4.68	5.87

All these results suggest a different enhancement mechanism only for the low concentrations, inducing the levelling-off of the difference between the two configurations. Most likely, different factors could contribute to the observed trends. First, an influence of the steric hindrance for the miRNA labelled at the 3' terminus is expected (as discussed in section 3.3). Such effect could be particularly detrimental in the case of low concentrations approaching the values of the dissociation constants between the probe and the miRNA, which are expected to be in the nM range.[45] Moreover, a second and probably dominant contribution can be ascribed to the SERS-active nanostructures themselves. In fact, at high miR-222 concentration it is expected that all the NPs are able to provide a sufficient electromagnetic field amplification, through the excitation of their Localized Surface Plasmon Resonances, to observe a SERS signal from the quite large population of miRNA-probe hybrids probed by the laser beam. In contrast, if few miRNA molecules are captured from the incubation solution, only the most efficient Raman hot-spots will be able to provide the needed enhancement.

3.2 Electromagnetic near field analysis for Ag-pSi nanostructures

FEM simulations were performed to corroborate such hypothesis by analysing the electric near-field (NF) intensity profiles inside and outside the gap of a dimer of Ag hemispheres in contact with the pSi surface, which was selected as simplified model of our plasmonic nanostructures. Based on the morphological parameters extracted from the FESEM analyses of the Ag-pSi-PDMS substrates, different NPs diameters (25-30-35 nm), centred at the average one, were considered for the simulations. For each diameter, gap values were varied between 2 nm and 8 nm, with a 2 nm step. Very small gaps (< 2 nm) were excluded from the studied range, as they can hardly accommodate the probe-miRNA hybrid, even if horizontally adsorbed on the NP surface, while 6 and 8 nm are expected to provide enough space for a successful hybridization. Representative

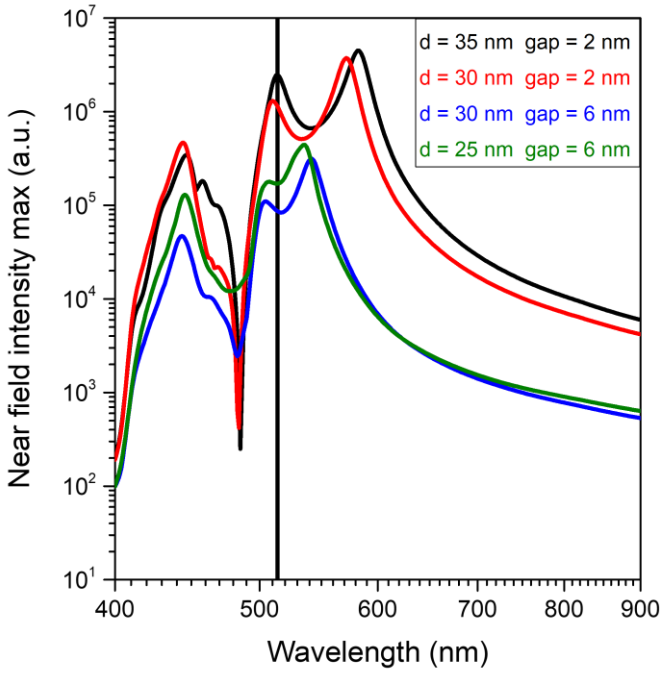

Figure 4. Maximum electric NF intensity calculated within the gap of a dimer of Ag hemispheres on a pSi surface by FEM simulations for different wavelengths and diameter-gap combinations of the AgNPs. The black vertical bar at 514.5 nm represents the excitation wavelength used for the SERS measurements.

spectra reporting the maximum electric NF intensity calculated within the gap between the Ag hemispheres are shown in Figure 4. All the spectra are featured by multiple resonances that extend towards wavelengths larger than the one of the excitation laser line, decreasing the inter-particle gap size and increasing the particle diameter, in agreement with the previous literature[46,47]. The highest NF intensity is observed for the longest wavelength resonance, located between 500 and 600 nm, depending on the size-gap combination. Moreover, it should be noted that most of the simulated dimers present an intense band around the excitation wavelength used for the SERS measurements (514.5 nm), supporting the well-known high efficiency of the Ag-pSi-PDMS substrates under green light excitation. Such resonance seems to originate from a splitting of the

main one due to inter-particle coupling when the gap becomes smaller and smaller, as suggested by their partial convolution for the largest gap –smallest diameter pairs. Panel a) and b) in Figure 5 show instead the profiles of the electric NF intensity at 514.5 nm extracted at different position within and outside the gap. R = 15 nm and G = 6 nm were selected as the most representative particles radius and gap size for the investigated system.

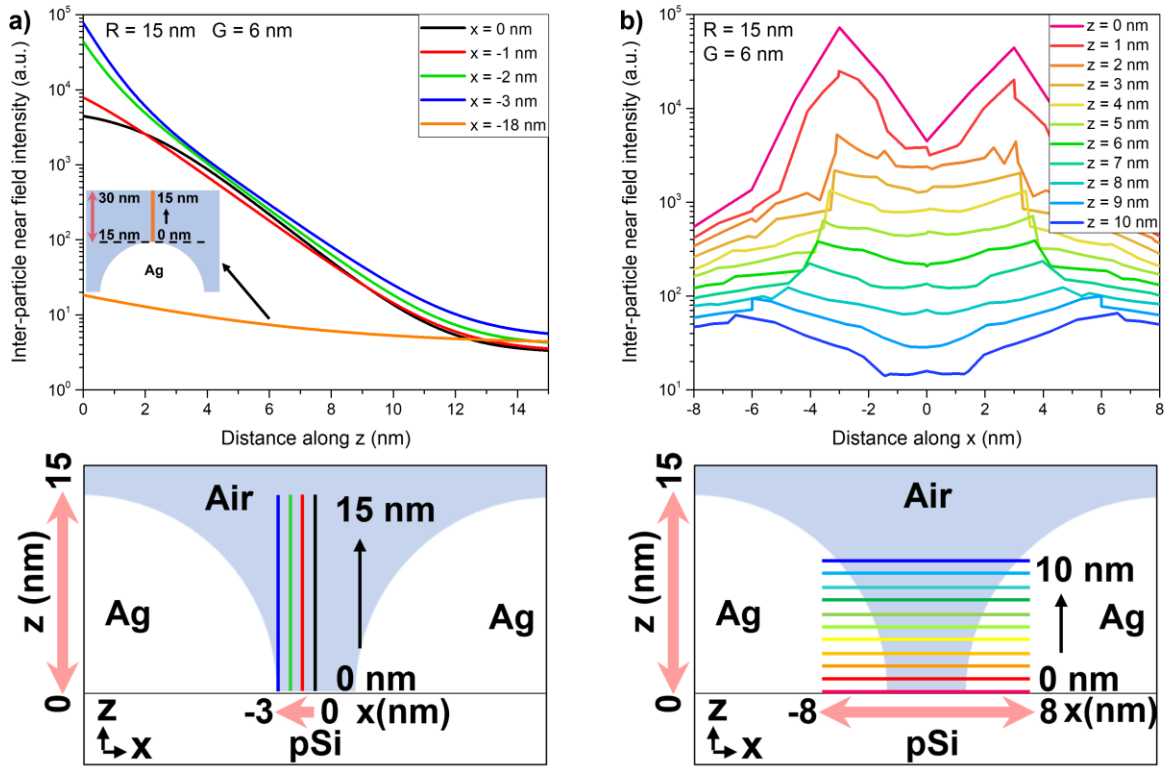

Figure 5. Spatial profiles of the electric NF intensity calculated within the gap (G = 6 nm) of a dimer of Ag hemispheres (R = 15 nm) on a pSi surface by FEM simulations a) along the z direction and b) along the x direction. The excitation wavelength was set at 514.5 nm. The inset in panel a) shows a z profile taken outside the gap (at x = -18 nm and z from 15 to 30 nm above the pSi surface).

For what concerns the z profiles, shown in panel a), the electric NF decays by order of magnitudes moving from z = 0 nm (the pSi surface level) to 15 nm. Curves extracted at different x location (x = 0 corresponds to the gap centre) feature different trends only for very short distances from the pSi surface: in such range the highest intensities and the fastest decrease are observed close to the AgNP surface (x = -2, -3 nm), while the maximum NF intensity is reduced but decays at a decreased rate if the profile is taken near the gap centre. The described trend is more pronounced when the gap becomes larger, with respect to the NP size (Figure S9), but, as anticipated, the differences strongly reduce at z > 2 nm for all gap-size combinations. The slight variation of the electric NF intensity along the interparticle axis beyond z = 3 nm can be better appreciated from the x profiles obtained at different z values reported in panel b) of Figure 5, where the symmetry of the NF intensity distribution with respect to the inter-particle gap center is verified.

Some significant differences between the electric NF intensities at the gap centre and edges appear again for quite high z values (> 9 nm), when the distance between the NPs surfaces is 12 nm. An interparticle separation of the order of the particle radius is indeed considered the cut-off beyond which interparticle coupling contribution cease to dominate.[48] The inset in panel a) of Figure 5 finally shows a z profile taken outside the gap (from the top of one of the particles, at x = -18 nm, z from 15 to 30 nm). Here, as expected, the electric NF intensity is several orders of magnitude lower than in the gap and monotonically decreases while the distance from the Ag hemisphere increases. It can be concluded that, in the case of a probe-miRNA hybrid in an interparticle gap, a Raman reporter is expected to benefit from a different enhancement depending on its position along the probe only if the oligo is bound to the NP very close to the Ag/pSi interface. Instead for $z \geq 3$ nm, the most likely situation, the electric NF experienced by the dye molecule is nearly constant throughout the gap at fixed z. At higher z values, some limited differences may however

arise due to the tilted orientation of the hybrids in an upright conformation with respect to the pSi surface. Outside the gap, instead, the SERS enhancement at 7.5 nm from the NP surface is reduced to about the 15% of the one observed at 1 nm spacing. The scheme in Figure 6, representing miRNA molecules hybridized to the probe-222 in or outside the gap between two AgNPs on a pSi surface, highlights the difference in the experienced NF intensity that characterizes the reporter in the 5' and 3' configurations outside the gap. However, as the electric field distribution is rather homogenous in the gap between the NPs, the beneficial effects of decreasing the reporter-to-surface distance are strongly reduced or even cancelled depending on the specific combination of NP diameter, gap size and binding site of the probe. Indeed, it should be underlined that the heterogeneity in the morphology of the SERS substrate, even if limited, can obviously affect the enhancement of the SERS signal obtained when the reporter at the 5'- terminus of the miRNA is located in the gap. Indeed, the reporter can be even in contact with the neighbouring NP in some cases. Unfortunately, the prevalence of the gap contribution to the SERS signal at low miRNA concentration does not allow the expected improvement of the LODs moving from the far- to the close-to-the-surface reporter configuration.

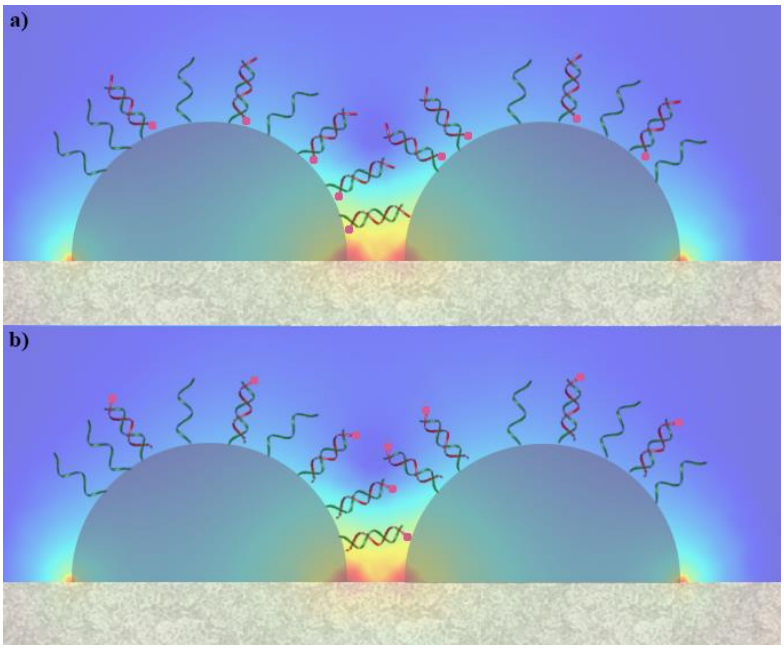

Figure 6. Scheme representing miRNA molecules hybridized to the probe-222 in or outside the gap between two AgNPs (R= 15 nm, G= 6 nm) on a pSi surface for both the a) 3' and 5') configurations of the Raman reporters. The calculated distribution of the electromagnetic near field around the dimer excited at 514.5 nm is reported as background.

Though, it should be noted that at the same time, the signal is already boosted in the gap for the miRNA R-5' configuration at low concentrations. As a result, the slope of the calibration curve is usually reduced compared to the high concentration regime (see Table S4). A further indication of a distinct origin of the SERS enhancement for the high and low concentrations of target miRNA is indeed provided by the non-linear trend often observed in SERS calibrations. In fact, the sensitivity should change if all the particles or only the hot-spots contribute to the SERS intensity. Modelling this variation is a great challenge, due to the strong dependence of such effects on the SERS substrate morphology. Nevertheless, some attempts to use non-linear fitting functions, such as the Langmuir or dose-response curves can be found in the literature.[49,50] Actually, none of the

two models provided a satisfactory fit of the current data, showing that adsorption models are not always adequate to describe the trend of the SERS intensity vs. the analyte concentration, probably because they do not take into account such hot-spot related effect that becomes evident only for very low concentrations of the target analyte. It should be mentioned that similar non-linearities were in many cases attributed to the SERS intensity fluctuations due to single molecule events in the nanomolar and subnanomolar concentration range.[1] Namely, it is assumed that such fluctuations depend on the motion of the analyte in and outside the available hot-spot, whose volume sharply decreases for increasing enhancement.[3] Though, such phenomena shouldn't be the source of non-linearity in the presented system, since the functionalization of the surface does not allow great motion of the involved molecules and the SERS measurements are not acquired in solution, where some dynamic equilibrium between bound and free miRNA could establish. Last, even the moderate dependence of the SERS intensity on the reporter position for the non-resonant Cy5 is compatible with the described mechanism. Indeed, if the Raman cross-section of the reporter is reduced, an increased plasmonic enhancement is needed to detect the probe-miRNA hybridization in the same miRNA concentration range. As a consequence, it can be speculated that the hot-spot contribution becomes dominant at higher miR-222 concentrations compared with the case of Cy3 and RGX, in agreement with the reduced differences between the 5' and 3' configurations and with the linear range extending towards high miRNA concentrations in case of the Cy5 reporter (up to 50 nM). Consistently, the comparison between the sensitivities calculated for the analysed configurations at high and low miR-222 concentration (Table S4) shows a remarkable variation of the slope of the regression lines in the two concentration regimes in the case of the resonant reporters, but a single sensitivity value for the Cy5 reporter.

3.3 Two-step assay: half2 R-3’ vs. half2 R-5’

Different concentrations of unlabelled miR-222 were incubated on the half1 functionalized SERS substrates and afterwards detected through the hybridization with the half2 probe labelled with the different reporters both at the 3’ or 5’ terminus. The results of the SERS maps acquired on the described samples are displayed in Figure 7 for the 5’ and 3’ RGX-labelled half2 probe.

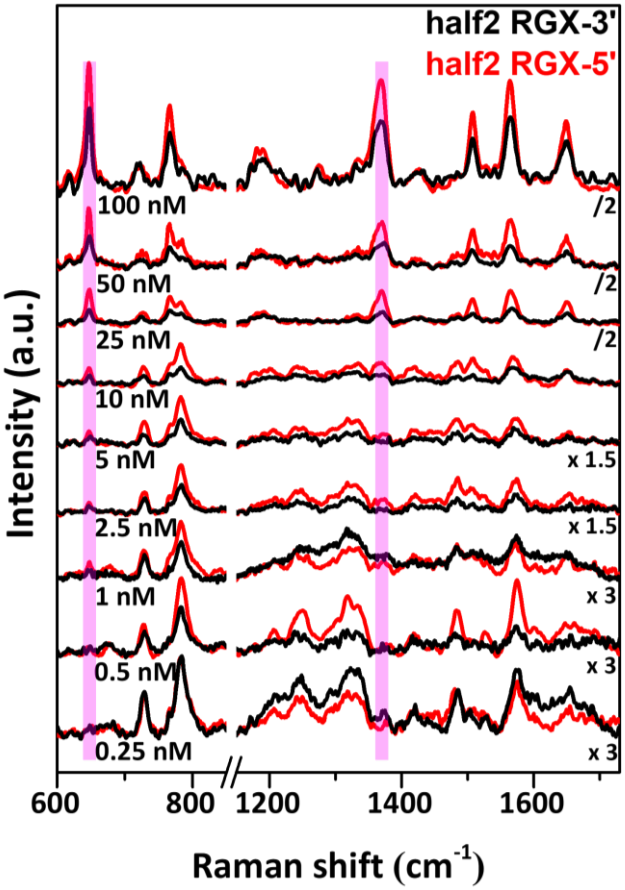

Figure 7. Average SERS spectra obtained from maps on the SERS substrate functionalized with half1, exposed to different concentrations of miR-222 and then incubated with half2-RGX-3’ (black curves) and half2 RGX-5’ (red curves), according to the two-step hybridization protocol. The violet bars highlight the two main bands of RGX (at 647 and 1364 cm^{-1}).

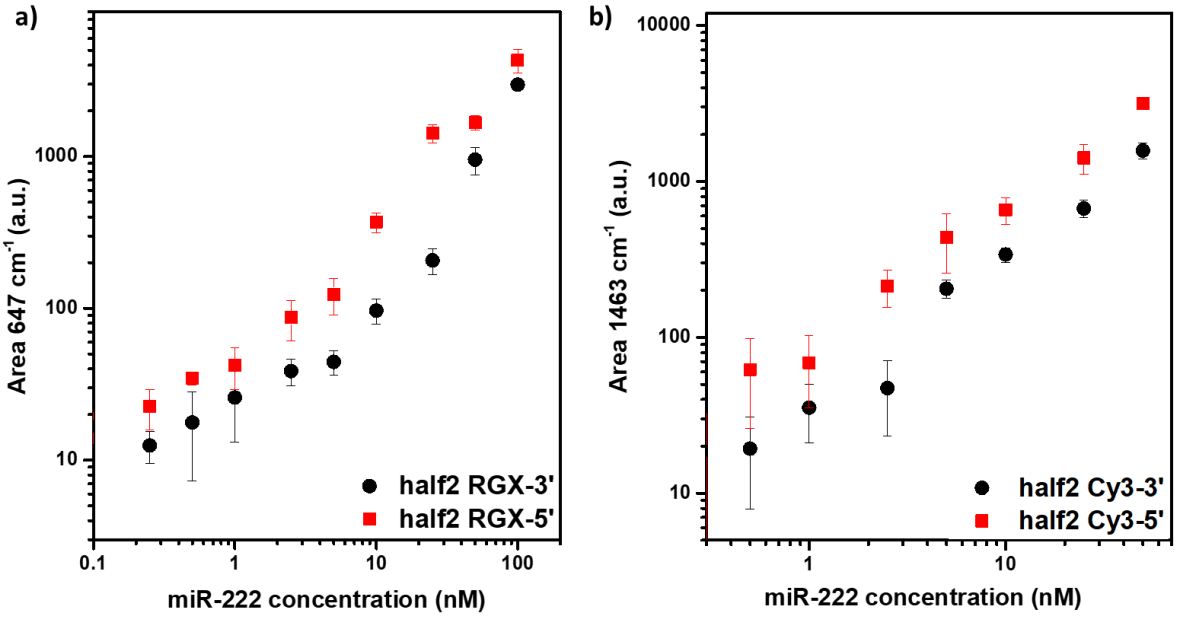

Figure 8. Average area of the main vibrational band of the half2 R-5'/3' vs. miR-222 concentration obtained by SERS mapping of the substrates functionalized according to the two-step assay. a) RGX and b) Cy3 were employed as Raman reporters. Red squares represent the close-to-the-surface (5') configuration, while black circles the far-from-the-surface (3') one. The error bars correspond to the standard deviations of 100 SERS measurements.

As expected, due to the reduced difference in the reporter-to-surface distance (3.5 nm vs. 7.5 instead of < 1 nm vs. 7.5 in the case of the labelled miR-222), in the two configurations the SERS intensity was only moderately enhanced when the reporter was located close to the AgNPs (generally less than 2 times the area of the Raman band of RGX at 647 cm^{-1} calculated for the 3' labelling). Differently from the case of the one-step assay, such enhancement does not fade for concentrations lower than 5 nM. A close inspection of the superimposed average SERS spectra (Figure S10 and S11a) highlights that some differences between the two configurations are preserved in most cases also below 10 nM miRNA concentration for the resonant reporters. Such

trend is also confirmed by the calibration curves of SERS area vs. miR-222 concentrations (Figure 8), which were derived by considering the integrated area of the same SERS bands analysed for the one-step assay. This outcome is reflected in the calculated LODs, which result 1506 pM and 357 pM when the half2 RGX-3' and the half2 RGX-5' are concerned, respectively. As evidenced by the experimental data, a systematic improvement of the sensitivity of the assay is achieved for the two-step assay by moving the reporter towards the surface of NPs, despite the order of magnitude of the LOD doesn't change. It should be noted that a similar benefit is obtained using the half2-Cy3, for which the LODs are 988 nM and 627 pM, as listed in Table 2.

Table 2. Limits Of Detection for the two-step assay performed by exploiting the six different configurations along with the miR-222 concentration ranges used for the linear regression. The calibration curves employed for the calculation of the LODs are shown in Figure S12.

	RGX		Cy3		Cy5	
	3'	5'	3'	5'	3'	5'
Linear range (nM)	0 - 10	0 – 10	0 - 10	0 - 10	0 - 50	0 - 25
R^2	0.943	0.977	0.952	0.979	0.968	0.979
LOD (nM)	1.51	0.357	0.988	0.627	17.5	7.05

Again, Cy5 provides the weakest SERS signal and the worst sensitivity. Despite the slight difference between the SERS intensity of the two configurations (Figure S11b and S13), the calculated LODs reveal an improved performance for the close-to-the-surface configuration.

The inspection of the regression parameters (Table S5) confirms a change of the sensitivity between the high and low concentration regime for the RGX reporter, but the phenomenon is mitigated in the case of Cy3. Unlike in the case of the one-step assay, however, the sensitivity for

the close-to-the surface configuration remains higher than for the far-from-the surface one. Moreover, the differences between the two configurations resulted statistically significant also in the low concentration range (95% confidence level, as shown in Table S6). Actually, the behaviour of the compared configurations appears to be different from the one detected in the one-step assay, as confirmed by the repetition of the experiments. However, such discrepancies cannot depend on a diverse electromagnetic enhancement mechanism: hot-spot contribution should again dominate at low miR-222 concentration. It can be therefore hypothesized that they depend on the impact of the position of probe/miRNA labelling on the hybridisation efficiency. Indeed, it is well known that steric hindrance effects play a significant role in duplex formation when the hybridization involves a surface-immobilized probe, such as in microarrays[51,52]. As an example, an excessive packing of probes at the surface is detrimental, since it results in slow hybridization kinetics and lowered degree of probe/target hybridization.[51,53] Moreover, it was observed that the hybridisation efficiency increases when probe-target binding occurs farther from the support surface, due to an improved accessibility of the oligonucleotide sequence.[54] For this reason, spacers are often employed to increase the distance of the strand and reduce steric interference from the support.[54] In such a framework, the presence of a bulky reporter at the close-to-the surface terminus of the half2 probe or miR-222 is expected to enhance steric hindrance related issues more than in the far-from the surface configurations. However, if the one-step and two-step assay are compared, it is immediately apparent that the half2 R-5'/miR-222 hybridization occurs in a less sterically hindered environment than the miRNA R-3'/probe-222 heteroduplex formation. Indeed, in the two-step assay, the second hybridization takes place at an increased distance from the NP surface. It is therefore reasonable that the observed trends arise from the combination of electromagnetic and hybridisation efficiency effects: the electromagnetic NF intensity dependence on the reporter-to-

surface distance strongly reduces in the low concentration regime for all the tested configurations, but the higher LODs for the miRNA R-3' configuration compared to those for the miRNA R-5' one are probably ascribable to the severe steric hindrance effects in the first case. It should be underlined, that the influence of steric constraints would probably not be appreciated in the absence of the levelling off of the electromagnetic enhancement. Instead, for the two-step assay, where steric issues concerning the reporter are relaxed for the second hybridization step, a slightly higher SERS intensity is still observed at low miR-222 concentration for the close-to- the surface configuration compared to the 3' one. It should be noted, indeed, that the inherent lower melting temperature of the half1-miRNA and miRNA-half2 complexes compared to the longer and thus more stable probe-222-miR-222 duplex was previously compensated by the optimization of the hybridization conditions[7]. Lastly, the existence of a relationship between the size of the reporters and the performance of the one-step assay in the 3' and 5' configurations agrees with the possible role of steric hindrance in determining the discussed results. In fact, the geometrical descriptors concerning molecular size reported in Table S3 point to RGX as the bulkiest reporter, in agreement with the reduced difference between the SERS intensity obtained for the assays performed in the close-to- and far-from-the surface configurations at high miR-222 concentrations compared to Cy3. Moreover, the enhanced steric issues due to the greater size of RGX compared with Cy3 could also explain the inversion of the LODs for the 5' and 3' configurations that is detected only for the RGX molecule.

Despite lower than initially expected, due to the described increased contribution of hot-spots to the SERS signal observed at low target concentrations, an increase of the sensitivity of the two-step protocol for miRNA detection is attained by reducing the distance between the reporter and

the plasmonic NPs. Such improvement can be fruitfully exploited to enhance the detection of such biomarkers in real samples.

4 Conclusions

Ag-porous silicon-PDMS SERS substrates were exploited to investigate the impact of the Raman reporter position along the sequence of oligo probes/targets on the sensitivity of a one-step and a two-step hybridization assay for the SERS detection of miRNAs. Such an aspect was indeed not evaluated in previous SERS studies exploiting labelled DNA probes for the detection of oligonucleotide targets.[12,16] Here, three reporters (RGX, Cy3 and Cy5) differing in size and electronic resonance were studied. As for the one-step assay, a significant variation (more than 6.5 nm) of the reporter-to-surface distance could be obtained by labelling the miRNA at the 3' and 5' terminus. The SERS analysis of several miR-222 R-5'/3' concentrations showed a clearly greater SERS intensity for the 3' configuration compared to the 5' one at concentrations above 5 nM; such improved SERS detection gradually vanished at lower miRNA concentrations. FEM simulations of the electric near field for a model Ag dimer on a pSi surface suggested that the unexpected concentration-dependent outcome could be compatible with an increased hot-spot contribution to the whole SERS signal in the nanomolar range of miR-222 concentrations. On the other side, for the two-step assay, a change in the reporter-to-surface spacing of about 4 nm was possible, by labelling the second half2 probe at the 3' or 5' terminus. The reduced variation of the reporter-to-surface distance between the two detection configurations yielded a mitigated difference between the SERS intensity observed for the two labelling positions. Interestingly, the LOD for miR-222 was always lowered for the close-to-the-surface configuration, in contrast to the case of the one-step assay. Such result points out the possible role of steric hindrance in decreasing the

hybridization efficiency in the case of the 3' labelled miRNA. On the whole, the study allowed to improve the sensitivity of the two-step assay and provided new insight on the complex balance between plasmonic effects and surface chemistry in the definition of the performance of a SERS bioassay.

Acknowledgements

Financial support from the POR FESR 2014-2020 Piedmont Regional Projects "Digital Technology For Lung Cancer Treatment"—DEFLECT (2018–2022) and from the PNRR grant agreement no. ECS00000036 (NODES) is gratefully acknowledged. We gratefully acknowledge Dexmet Corporation for providing the copper grids used for the FESEM imaging.

References

(1) Langer, J.; de Aberasturi, D. J.; Aizpurua, J.; Alvarez-Puebla, R. A.; Auguié, B.; Baumberg, J. J.; Bazan, G. C.; Bell, S. E. J.; Boisen, A.; Brolo, A. G.; Choo, J.; Cialla-May, D.; Deckert, V.; Fabris, L.; Faulds, K.; Javier García de Abajo, F.; Goodacre, R.; Graham, D.; Haes, A. J.; Haynes, C. L.; Huck, C.; Itoh, T.; Käll, M.; Kneipp, J.; Kotov, N. A.; Kuang, H.; Le Ru, E. C.; Lee, H. K.; Li, J. F.; Ling, X. Y.; Maier, S. A.; Mayerhöfer, T.; Moskovits, M.; Murakoshi, K.; Nam, J. M.; Nie, S.; Ozaki, Y.; Pastoriza-Santos, I.; Perez-Juste, J.; Popp, J.; Pucci, A.; Reich, S.; Ren, B.; Schatz, G. C.; Shegai, T.; Schlücker, S.; Tay, L. L.; George Thomas, K.; Tian, Z. Q.; van Duyne, R. P.; Vo-Dinh, T.; Wang, Y.; Willets, K. A.; Xu, C.; Xu, H.; Xu, Y.; Yamamoto, Y. S.; Zhao, B.; Liz-Marzán, L. M. Present and Future of Surface-Enhanced Raman Scattering. *ACS Nano*. American Chemical Society January 28, 2020, pp 28–117. https://doi.org/10.1021/acsnano.9b04224.

(2) Lee, H. K.; Lee, Y. H.; Koh, C. S. L.; Phan-Quang, G. C.; Han, X.; Lay, C. L.; Sim, H. Y. F.; Kao, Y. C.; An, Q.; Ling, X. Y. Designing Surface-Enhanced Raman Scattering (SERS) Platforms beyond Hotspot Engineering: Emerging Opportunities in Analyte Manipulations and Hybrid Materials. *Chemical Society Reviews*. Royal Society of Chemistry February 7, 2019, pp 731–756. https://doi.org/10.1039/c7cs00786h.

(3) Zong, C.; Xu, M.; Xu, L. J.; Wei, T.; Ma, X.; Zheng, X. S.; Hu, R.; Ren, B. Surface-Enhanced Raman Spectroscopy for Bioanalysis: Reliability and Challenges. *Chemical Reviews*. American Chemical Society May 23, 2018, pp 4946–4980. https://doi.org/10.1021/acs.chemrev.7b00668.

(4) Muhammad, M.; Huang, Q. A Review of Aptamer-Based SERS Biosensors: Design Strategies and Applications. *Talanta*. Elsevier B.V. May 15, 2021. https://doi.org/10.1016/j.talanta.2021.122188.

(5) Lussier, F.; Thibault, V.; Charron, B.; Wallace, G. Q.; Masson, J. F. Deep Learning and Artificial Intelligence Methods for Raman and Surface-Enhanced Raman Scattering. *TrAC - Trends in Analytical Chemistry*. Elsevier B.V. March 1, 2020. https://doi.org/10.1016/j.trac.2019.115796.

(6) Peng, L.; Zhou, J.; Liang, Z.; Zhang, Y.; Petti, L.; Jiang, T.; Gu, C.; Yang, D.; Mormile, P. SERS-Based Sandwich Bioassay Protocol of MiRNA-21 Using Au@Ag Core-Shell Nanoparticles and a Ag/TiO2 Nanowires Substrate. *Analytical Methods* **2019**, *11* (23), 2960–2968. https://doi.org/10.1039/c9ay00573k.

(7) Novara, C.; Chiadò, A.; Paccotti, N.; Catuogno, S.; Esposito, C. L.; Condorelli, G.; de Franciscis, V.; Geobaldo, F.; Rivolo, P.; Giorgis, F. SERS-Active Metal-Dielectric Nanostructures Integrated in Microfluidic Devices for Label-Free Quantitative Detection of MiRNA. *Faraday Discuss* **2017**, *205*, 271–289. https://doi.org/10.1039/C7FD00140A.

(8) Jet, T.; Gines, G.; Rondelez, Y.; Taly, V. Advances in Multiplexed Techniques for the Detection and Quantification of MicroRNAs. *Chemical Society Reviews*. Royal Society of Chemistry March 21, 2021, pp 4141–4161. https://doi.org/10.1039/d0cs00609b.

(9) Condrat, C. E.; Thompson, D. C.; Barbu, M. G.; Bugnar, O. L.; Boboc, A.; Cretoiu, D.; Suciu, N.; Cretoiu, S. M.; Voinea, S. C. MiRNAs as Biomarkers in Disease: Latest Findings Regarding Their Role in Diagnosis and Prognosis. *Cells*. NLM (Medline) January 23, 2020. https://doi.org/10.3390/cells9020276.

(10) Bertone, S.; Calmo, R.; Chiadò, A. Detection Methodologies for MicroRNA Biomarker Profiling. In *MicroRNA: From Bench to Bedside*; Academic Press, 2022; pp 217–240. https://doi.org/10.1016/B978-0-323-89774-7.00029-7.

(11) Zheng, J.; Ma, D.; Shi, M.; Bai, J.; Li, Y.; Yang, J.; Yang, R. A New Enzyme-Free Quadratic SERS Signal Amplification Approach for Circulating MicroRNA Detection in Human Serum. *Chemical Communications* **2015**, *51* (90), 16271–16274. https://doi.org/10.1039/c5cc06549f.

(12) Wu, L.; Dias, A.; Diéguez, L. Surface Enhanced Raman Spectroscopy for Tumor Nucleic Acid: Towards Cancer Diagnosis and Precision Medicine. *Biosensors and Bioelectronics*. Elsevier Ltd May 15, 2022. https://doi.org/10.1016/j.bios.2022.114075.

(13) He, Y.; Yang, X.; Yuan, R.; Chai, Y. Switchable Target-Responsive 3D DNA Hydrogels As a Signal Amplification Strategy Combining with SERS Technique for Ultrasensitive Detection of MiRNA 155. *Anal Chem* **2017**, *89* (16), 8538–8544. https://doi.org/10.1021/acs.analchem.7b02321.

(14) Wang, Z.; Ye, S.; Zhang, N.; Liu, X.; Wang, M. Triggerable Mutually Amplified Signal Probe Based SERS-Microfluidics Platform for the Efficient Enrichment and Quantitative

Detection of MiRNA. *Anal Chem* **2019**, *91* (8), 5043–5050. https://doi.org/10.1021/acs.analchem.8b05172.

(15) Schlücker, S. Surface-Enhanced Raman Spectroscopy: Concepts and Chemical Applications. *Angewandte Chemie - International Edition*. Wiley-VCH Verlag May 5, 2014, pp 4756–4795. https://doi.org/10.1002/anie.201205748.

(16) Pala, L.; Mabbott, S.; Faulds, K.; Bedics, M. A.; Detty, M. R.; Graham, D. Introducing 12 New Dyes for Use with Oligonucleotide Functionalised Silver Nanoparticles for DNA Detection with SERS. *RSC Adv* **2018**, *8* (32), 17685–17693. https://doi.org/10.1039/c8ra01998c.

(17) Song, Y.; Xu, T.; Xu, L. P.; Zhang, X. Superwettable Nanodendritic Gold Substrates for Direct MiRNA SERS Detection. *Nanoscale* **2018**, *10* (45), 20990–20994. https://doi.org/10.1039/c8nr07348a.

(18) Zhang, N.; Ye, S.; Wang, Z.; Li, R.; Wang, M. A Dual-Signal Twinkling Probe for Fluorescence-SERS Dual Spectrum Imaging and Detection of MiRNA in Single Living Cell via Absolute Value Coupling of Reciprocal Signals. *ACS Sens* **2019**, *4* (4), 924–930. https://doi.org/10.1021/acssensors.9b00031.

(19) Yang, C. J.; Shen, W. G.; Liu, C. J.; Chen, Y. W.; Lu, H. H.; Tsai, M. M.; Lin, S. C. MiR-221 and MiR-222 Expression Increased the Growth and Tumorigenesis of Oral Carcinoma Cells. *Journal of Oral Pathology and Medicine* **2011**, *40* (7), 560–566. https://doi.org/10.1111/j.1600-0714.2010.01005.x.

(20) Bettazzi, F.; Hamid-Asl, E.; Esposito, C. L.; Quintavalle, C.; Formisano, N.; Laschi, S.; Catuogno, S.; Iaboni, M.; Marrazza, G.; Mascini, M.; Cerchia, L.; De Franciscis, V.; Condorelli, G.; Palchetti, I. Electrochemical Detection of MiRNA-222 by Use of a Magnetic Bead-Based Bioassay. *Anal Bioanal Chem* **2013**, *405* (2–3), 1025–1034. https://doi.org/10.1007/s00216-012-6476-7.

(21) Li, S.; Yan, G.; Yue, M.; Wang, L. Extracellular Vesicles-Derived MicroRNA-222 Promotes Immune Escape via Interacting with ATF3 to Regulate AKT1 Transcription in Colorectal Cancer. *BMC Cancer* **2021**, *21*, 349. https://doi.org/10.1186/s12885-021-08063-5.

(22) Ravegnini, G.; Cargnin, S.; Sammarini, G.; Zanotti, F.; Bermejo, J. L.; Hrelia, P.; Terrazzino, S.; Angelini, S. Prognostic Role of MiR-221 and MiR-222 Expression in Cancer Patients: A Systematic Review and Meta-Analysis. *Cancers*. MDPI AG July 1, 2019, p 970. https://doi.org/10.3390/cancers11070970.

(23) Song, Q.; An, Q.; Niu, B.; Lu, X.; Zhang, N.; Cao, X. Role of MiR-221/222 in Tumor Development and the Underlying Mechanism. *J Oncol* **2019**, *2019*, 7252013. https://doi.org/10.1155/2019/7252013.

(24) Di Martino, M. T.; Arbitrio, M.; Caracciolo, D.; Cordua, A.; Cuomo, O.; Grillone, K.; Riillo, C.; Caridà, G.; Scionti, F.; Labanca, C.; Romeo, C.; Siciliano, M. A.; D'Apolito, M.; Napoli, C.; Montesano, M.; Farenza, V.; Uppolo, V.; Tafuni, M.; Falcone, F.; D'Aquino,

G.; Calandruccio, N. D.; Luciano, F.; Pensabene, L.; Tagliaferri, P.; Tassone, P. MiR-221/222 as Biomarkers and Targets for Therapeutic Intervention on Cancer and Other Diseases: A Systematic Review. *Molecular Therapy - Nucleic Acids*. Cell Press March 8, 2022, pp 1191–1224. https://doi.org/10.1016/j.omtn.2022.02.005.

(25) Wang, D.; Sang, Y.; Sun, T.; Kong, P.; Zhang, L.; Dai, Y.; Cao, Y.; Tao, Z.; Liu, W. Emerging Roles and Mechanisms of MicroRNA-222-3p in Human Cancer. *International Journal of Oncology*. Spandidos Publications May 1, 2021, p 20. https://doi.org/10.3892/IJO.2021.5200.

(26) Garofalo, M.; Quintavalle, C.; Romano, G.; M. Croce, C.; Condorelli, G. MiR221/222 in Cancer: Their Role in Tumor Progression and Response to Therapy. *Curr Mol Med* **2011**, *12* (1), 27–33. https://doi.org/10.2174/156652412798376170.

(27) Medina, R.; Zaidi, S. K.; Liu, C. G.; Stein, J. L.; VanWijnen, A. J.; Croce, C. M.; Stein, G. S. MicroRNAs 221 and 222 Bypass Quiescence and Compromise Cell Survival. *Cancer Res* **2008**, *68* (8), 2773–2780. https://doi.org/10.1158/0008-5472.CAN-07-6754.

(28) Chiadò, A.; Novara, C.; Lamberti, A.; Geobaldo, F.; Giorgis, F.; Rivolo, P. Immobilization of Oligonucleotides on Metal-Dielectric Nanostructures for MiRNA Detection. *Anal Chem* **2016**, *88* (19). https://doi.org/10.1021/acs.analchem.6b02186.

(29) Pettersen, E. F.; Goddard, T. D.; Huang, C. C.; Couch, G. S.; Greenblatt, D. M.; Meng, E. C.; Ferrin, T. E. UCSF Chimera—A Visualization System for Exploratory Research and Analysis. *J Comput Chem* **2004**, *25* (13), 1605–1612. https://doi.org/10.1002/JCC.20084.

(30) Palmara, G.; Chiadò, A.; Calmo, R.; Ricciardi, C. Succinic Anhydride Functionalized Microcantilevers for Protein Immobilization and Quantification. *Anal Bioanal Chem* **2016**, *408* (28), 7917–7926. https://doi.org/10.1007/S00216-016-9920-2/FIGURES/3.

(31) Beleites, C.; Sergo, V. HyperSpec: A Package to Handle Hyperspectral Data Sets in R. 2015. http://hyperspec.r-forge.r-project.org.

(32) Shrivastava, A.; Gupta, V. Methods for the Determination of Limit of Detection and Limit of Quantitation of the Analytical Methods. *Chronicles of Young Scientists* **2011**, *2* (1), 21. https://doi.org/10.4103/2229-5186.79345.

(33) Liu, F. M.; Köllensperger, P. A.; Green, M.; Cass, A. E. G.; Cohen, L. F. A Note on Distance Dependence in Surface Enhanced Raman Spectroscopy. *Chem Phys Lett* **2006**, *430*, 173–176.

(34) Hill, H. D.; Millstone, J. E.; Banholzer, M. J.; Mirkin, C. A. The Role Radius of Curvature Plays in Thiolated Oligonucleotide Loading on Gold Nanoparticles. *ACS Nano* **2009**, *3* (2), 418–424. https://doi.org/10.1021/nn800726e.

(35) Love, J. C.; Estroff, L. A.; Kriebel, J. K.; Nuzzo, R. G.; Whitesides, G. M. Self-Assembled Monolayers of Thiolates on Metals as a Form of Nanotechnology. *Chemical Reviews*. April 2005, pp 1103–1169. https://doi.org/10.1021/cr0300789.

(36) Marotta, N. E.; Beavers, K. R.; Bottomley, L. A. Limitations of Surface Enhanced Raman Scattering in Sensing DNA Hybridization Demonstrated by Label-Free DNA Oligos as Molecular Rulers of Distance-Dependent Enhancement. *Anal Chem* **2013**, *85* (3), 1440–1446. https://doi.org/10.1021/ac302454j.

(37) Barhoumi, A.; Zhang, D.; Halas, N. J. Barhoumi08_orient. *JACS* **2008**, *130*, 14040–14041.

(38) Saini, G. S. S.; Sharma, A.; Kaur, S.; Bindra, K. S.; Sathe, V.; Tripathi, S. K.; Mhahajan, C. G. Rhodamine 6G Interaction with Solvents Studied by Vibrational Spectroscopy and Density Functional Theory. *J Mol Struct* **2009**, *931* (1–3), 10–19. https://doi.org/10.1016/j.molstruc.2009.05.015.

(39) Masango, S. S.; Hackler, R. A.; Large, N.; Henry, A. I.; McAnally, M. O.; Schatz, G. C.; Stair, P. C.; Van Duyne, R. P. High-Resolution Distance Dependence Study of Surface-Enhanced Raman Scattering Enabled by Atomic Layer Deposition. *Nano Lett* **2016**, *16* (7), 4251–4259. https://doi.org/10.1021/acs.nanolett.6b01276.

(40) Kovacs, G. J.; Loutfy, R. 0; Vincett, P. S.; Jennings, C.; Aroca, R. Articles Distance Dependence of SERS Enhancement Factor from Langmuir-Blodgett Monolayers on Metal Island Films: Evidence for the Electromagnetic Mechanism. *Langmuir* **1986**, *2* (6), 689–694.

(41) Murray, C. A.; Allara, D. L. Measurement of the Molecule-Silver Separation Dependence of Surface Enhanced Raman Scattering in Multilayered Structures. *J Chem Phys* **1982**, *76* (3), 1290–1303. https://doi.org/10.1063/1.443101.

(42) Sato, H.; Kawasaki, M.; Kasatani, K.; Katsumata, M. Raman Spectra of Some Indo-, Thia- and Selena-Carbocyanine Dyes. *Journal of Raman Spectroscopy* **1988**, *19*, 129–132.

(43) Li, J. F.; Li, C. Y.; Aroca, R. F. Plasmon-Enhanced Fluorescence Spectroscopy. *Chemical Society Reviews*. Royal Society of Chemistry July 7, 2017, pp 3962–3979. https://doi.org/10.1039/c7cs00169j.

(44) Jahn, I. J.; Grjasnow, A.; John, H.; Weber, K.; Popp, J.; Hauswald, W. Noise Sources and Requirements for Confocal Raman Spectrometers in Biosensor Applications. *Sensors* **2021**, *21* (15). https://doi.org/10.3390/s21155067.

(45) Zhou, M.; Chen, X.; Yang, H.; Fang, X.; Gu, H.; Xu, H. Determination of the Binding Constant between Oligonucleotide-Coupled Magnetic Microspheres and Target DNA. *ACS Omega* **2019**, *4* (4), 6931–6938. https://doi.org/10.1021/acsomega.8b03654.

(46) le Ru, E. C.; Etchegoin, P. G. Phenomenological Local Field Enhancement Factor Distributions around Electromagnetic Hot Spots. *Journal of Chemical Physics* **2009**, *130* (18), 4–7. https://doi.org/10.1063/1.3138784.

(47) Novara, C.; Dalla Marta, S.; Virga, A.; Lamberti, A.; Angelini, A.; Chiadò, A.; Rivolo, P.; Geobaldo, F.; Sergo, V.; Bonifacio, A.; Giorgis, F. SERS-Active Ag Nanoparticles on Porous Silicon and PDMS Substrates: A Comparative Study of Uniformity and Raman

Efficiency. *Journal of Physical Chemistry C* **2016**, *120* (30). https://doi.org/10.1021/acs.jpcc.6b03852.

(48) Halas, N. J.; Lal, S.; Chang, W. S.; Link, S.; Nordlander, P. Plasmons in Strongly Coupled Metallic Nanostructures. *Chem Rev* **2011**, *111*, 3913–3961. https://doi.org/10.1021/cr200061k.

(49) Massarini, E.; Wästerby, P.; Landström, L.; Lejon, C.; Beck, O.; Andersson, P. O. Massarini LOD Langmuir. *Sens Actuators B Chem* **2015**, *207*, 437–446.

(50) Altun, A. O.; Bond, T.; Pronk, W.; Park, H. G. Sensitive Detection of Competitive Molecular Adsorption by Surface-Enhanced Raman Spectroscopy. *Langmuir* **2017**, *33* (28), 6999–7006. https://doi.org/10.1021/acs.langmuir.7b01186.

(51) Xu, F.; Pellino, A. M.; Knoll, W. Electrostatic Repulsion and Steric Hindrance Effects of Surface Probe Density on Deoxyribonucleic Acid (DNA)/Peptide Nucleic Acid (PNA) Hybridization. *Thin Solid Films* **2008**, *516* (23), 8634–8639. https://doi.org/10.1016/j.tsf.2008.06.067.

(52) Vanjur, L.; Carzaniga, T.; Casiraghi, L.; Chiari, M.; Zanchetta, G.; Buscaglia, M. Non-Langmuir Kinetics of DNA Surface Hybridization. *Biophys J* **2020**, *119* (5), 989–1001. https://doi.org/10.1016/j.bpj.2020.07.016.

(53) Peterson, A. W.; Heaton, R. J.; Georgiadis, R. M. The Effect of Surface Probe Density on DNA Hybridization. *Nucleic Acids Res* **2001**, *29* (24), 5163–5168.

(54) Shchepinov, M. S.; Case-Green, S. C.; Southern, E. M. Steric Factors Influencing Hybridisation of Nucleic Acids to Oligonucleotide Arrays. *Nucleic Acids Res* **1997**, *25* (6), 1155–1161. https://doi.org/10.1093/nar/25.6.1155.